PHYSICAL REVIEW B **83**, 115316 (2011)

Strong phase separation of strained $In_xGa_{1-x}N$ layers due to spinodal and binodal decomposition: Formation of stable quantum dots

C. Tessarek,[*] S. Figge, T. Aschenbrenner, S. Bley, A. Rosenauer, M. Seyfried, J. Kalden, K. Sebald,
J. Gutowski, and D. Hommel

Institute of Solid State Physics, University of Bremen, Otto-Hahn-Allee 1, D-28359 Bremen, Germany

(Received 3 August 2010; revised manuscript received 27 January 2011; published 14 March 2011)

InGaN quantum dots were grown by metal-organic vapor phase epitaxy using a phase-separation process based on spinodal and binodal decomposition. Uncapped structures were grown which show InGaN phases with two different In contents on the surface. The high-In-content phase accumulates to huge islands while the low-In content phase forms flat meander and quantum-dot-like structures on the surface. The dissolution of the high-In-containing phase is very sensitive to the growth temperature of the GaN capping while there is no significant change of the InGaN quantum dot structures. The samples were investigated with transmission and scanning electron microscopy, photoluminescence measurements, and x-ray diffraction. A narrow growth window concerning the $In_xGa_{1-x}N$ composition was found in which the formation of quantum dots takes place. This growth window is in good agreement with the InGaN miscibility gap calculated for a strained InGaN layer. A detailed theoretical discussion is presented and the quantum dot and island formation will be explained by a strain-modified spinodal and binodal decomposition model.

DOI: 10.1103/PhysRevB.83.115316 PACS number(s): 64.75.St, 78.67.Hc, 68.37.Hk, 68.37.Ma

I. INTRODUCTION

InGaN based quantum dots (QDs) are of high interest for applications in light emitting devices due to their predicted properties such as lower threshold current densities for laser diodes (LDs), better temperature stability for the luminescence intensity, and less nonradiative recombination in comparison to a quantum well (QW) system. Moreover, they would pave the way for applications such as quantum computing and quantum cryptography based on single photon emitters (SPEs). Promising results toward electrically driven SPE have been achieved in our institute as InGaN QDs in monolithic microcavities[1] and electroluminescence from a single QD.[2] Although some groups have reported on the growth of InGaN QDs via different growth techniques,[3,4] none have succeeded to grow an electrically driven QD-based LD. Still, all InGaN LDs are based on QW structures (e.g., [5,6]). For the growth of a homogeneous QW, it is desired to suppress the phase separation caused by spinodal and binodal decomposition.[7] Contrarily, one can take advantage of spinodal decomposition to grow InGaN QDs.

For other material systems such as InGaAs, growth of QDs via spinodal decomposition is already established.[8,9] For the InGaN material system, spinodal decomposition is a controversial issue. Although a spinodal phase diagram has been calculated for InGaN with a large unstable region at typical growth temperatures,[7] there are many experimental reports for InGaN growth almost over the full composition range.[10,11] This disagreement can be explained by the reduction of the unstable region due to strain in the InGaN layer caused by the GaN substrate.[12]

Here, we report on strong phase separation of the InGaN system that leads to QD-like structures. The experimental results are in agreement with theoretical predictions based on a strained InGaN layer. The insights obtained through this work concerning the realization of nanostructures are not limited to the InGaN material system only, but can also be applied to systems such as GaAsSb or CdZnTe. For these materials, a miscibility gap due to spinodal decomposition[13,14] has also been predicted. In the case of a layer on a substrate with a different lattice constant it is expected that the strain influences the spinodal phase diagram. QDs in other systems can be realized if the effective spinodal curve is known.

In the first part of this work some theoretical aspects will be discussed which are used later to understand and to interpret the experimental results. Based on a thermodynamic analysis[15] the indium incorporation from the gas phase into the InGaN solid was calculated. Spinodal and binodal lines for different strain states of InGaN on GaN will be presented. The pattern formation of InGaN after phase separation[16] will be discussed and expanded to the case of InGaN grown on GaN. Strain fields of a freestanding InGaN islands are calculated.

In the second part, results obtained on uncapped and capped InGaN structures are shown. With different measurement techniques, such as transmission and scanning electron microscopy (TEM and SEM, respectively), photoluminescence (PL), and x-ray diffraction (XRD), phase-separated $In_xGa_{1-x}N$ structures with high and low values of x were determined. The In-poor InGaN is forming flat QD-like and meandering structures while the In-rich InGaN accumulates to form large and high islands, following a Volmer-Weber growth mode. The evolution of these structures with time and thermal treatment is presented. Above a certain temperature the GaN capping of the InGaN structures leads to dissolution of large In-rich InGaN islands and incorporation of residuals into the GaN capping layer. In contrast, the GaN capping does not affect the In-poor InGaN dots or meanders. Furthermore, it will be shown that the density of QDs can be controlled by the growth temperature. A narrow $In/(In + Ga)$ composition range will be determined in which the formation of InGaN QDs takes place, being in good agreement with the spinodal lines calculated for strained InGaN. Finally, a QD formation model based on spinodal decomposition will be suggested.

II. EXPERIMENTAL

The samples were grown epitaxially in a Thomas Swan 3″ × 2″ vertical closed coupled shower head metal-organic vapor phase reactor. Trimethylindium (TMI), trimethylgallium (TMG), and ammonia (NH_3) were used as precursors. H_2 and N_2 were used as carrier gases. All samples were grown on 2-μm-thick *c*-plane Si-doped GaN templates deposited on sapphire substrates. The TMI flux was controlled with a velocity of sound measurement equipment (Epison III) to ensure a constant gas-flux rate.

Four series of samples were produced and investigated. First, uncapped InGaN structures were grown at 600 or 650 °C with an In/(In + Ga) gas-flux ratio of 82%. The intended layer thickness was 1.5 nm. After growth of the InGaN layer, each sample passed through a different annealing procedure.

Second, the influence of GaN capping on the InGaN structures was investigated. Two samples were capped with GaN grown at 700 and 750 °C, respectively. Furthermore, for both samples an additional high-temperature capping was performed[17] to obtain a high-quality GaN overlayer.

Third, InGaN layers were grown at 600, 650, and 700 °C to show the impact of the growth temperature on the QD density.

Fourth, to investigate the influence of the In concentration of an $In_xGa_{1-x}N$ layer with x inside and outside of the unstable region of a modified spinodal phase diagram for the fully strained case, five samples with x reaching from 0.73 to 0.92 were grown.

PL and μ-PL measurements were performed using a 325-nm HeCd gas laser or a 406-nm LD as excitation sources and a SPEX 270M or a SPEX 1704 spectrometer with a resolution of 170 μeV. Surface topography measurements were done with a Park Scientific Autoprobe CP atomic force microscope (AFM) in noncontact mode. XRD was measured with a Philips X'Pert MRD. SEM images were recorded using a FEI Nova Nanolab 200 DualBeam System. Scanning TEM (STEM) measurements were performed with a TITAN 80/300 TEM operated at 300 keV.

III. THEORETICAL BACKGROUND

To determine the indium incorporation from the gas phase into the InGaN solid, a thermodynamic analysis adapted from Koukitu *et al.*[15] was performed. This analysis is mainly based on the simplified assumption of a reversible chemical reaction between the gas phase and the solid:

$$M(\mathrm{g}) + \mathrm{NH_3(g)} \Leftrightarrow M\mathrm{N(s)} + \tfrac{3}{2}\mathrm{H_2(g)}, \tag{1}$$

with M representing In or Ga. The corresponding law of mass action is

$$K_M = \frac{a_{MN} P_{H_2}^{3/2}}{P_M P_{NH_3}}, \tag{2}$$

with K_M being the equilibrium constant, a_{MN} the activity, and P the partial pressures of each component. More details about this theory are given in Ref. 18. In Fig. 1 the composition x in the $In_xGa_{1-x}N$ solid is plotted versus the gas-phase ratio for different temperatures reaching from 600 to 800 °C. For the calculations, a pressure of 933 mbar, an N_2 and NH_3 flux of 5000 and 3000 sccm, respectively, and a total metal-organica flux of 35 μmol/min were used. A linearly temperature-dependent NH_3 dissociation of $\alpha = (0.0016\ \mathrm{K}^{-1})T - 1.19$ and an x-dependent interaction parameter[19] were assumed. A gas-phase ratio of In/(In + Ga) > 0.7 leads, below 700 °C, to a nearly linear relation between the gas-phase ratio and x. At 750 °C there is a slight decrease and, at 800 °C, there is a strong decrease of x for In/(In + Ga) > 0.7. At high temperature such as 800 °C and at high-indium content the solid composition is very sensitive to small changes of the temperature and gas-phase ratio. Considering this thermodynamical model only and neglecting other effects such as phase separation or composition pulling,[20] it can be concluded that, in the temperature regime below 700 °C, the gas-phase composition is nearly identical to the resulting composition of the solid. Therefore, the InGaN layers were grown at temperatures below 700 °C.

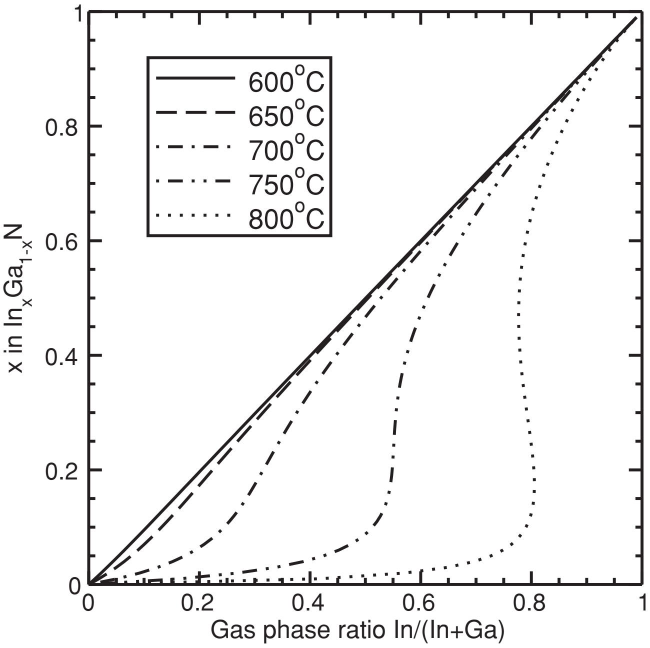

FIG. 1. Composition x in the $In_xGa_{1-x}N$ solid plotted versus the gas-phase ratio for temperatures from 600 to 800 °C. With a gas-phase ratio of In/(In + Ga) = 0.82, nearly the same composition is expected in the solid for growth temperatures below 700 °C.

Spinodal and binodal decomposition describes a phase-separation process of at least two compounds, which is a result of the minimization of the free energy of the system. A spinodal and binodal phase diagram can be calculated using the Gibbs function $G = H - TS$ of a system, with H being the enthalpy, S the entropy, and T the temperature of the system. The binodal line in the phase diagram denotes the absolute minima of the Gibbs function ($\partial G/\partial x = 0$). A separation into the binodal phases would result in the total minimization of the systems free energy. However, spontaneous phase separation cannot take place in concave regions of the Gibbs function $\partial^2 G/\partial^2 x > 0$, as this would lead locally to an increase in free energy. Thus, only within the limits of the spinodal separatrix $\partial^2 G/\partial^2 x = 0$ does spontaneous decomposition occur in the absence of nucleation centers and lead to a reduction of the free energy.[21]

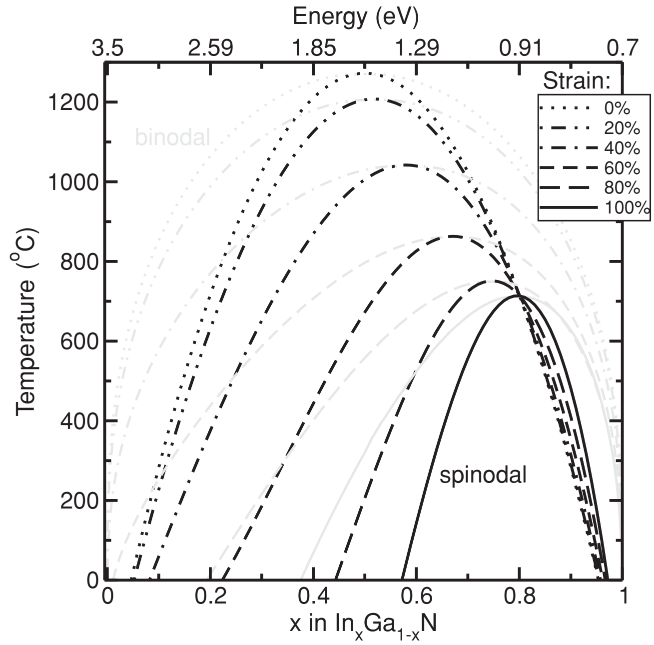

FIG. 2. Spinodal (black) and binodal (gray) lines calculated for different strain states of the InGaN layer on a GaN substrate. A strain state of 100% corresponds to pseudomorphic material grown on GaN, whereas 0% means completely relaxed material. With increasing strain in the InGaN layer, the critical temperature decreases and shifts toward higher x. Nevertheless, a miscibility gap exists for growth temperatures below 713 °C.

Ho and Stringfellow[7] have calculated a spinodal phase diagram for free-standing InGaN layer. However, for the growth of InGaN on GaN, strain in the InGaN layer has to be taken into account. In Fig. 2 the spinodal and binodal lines are depicted according to the theory from Karpov.[12] The calculations were performed considering InGaN on wurtzite c-plane GaN and an interaction constant of 25 700 J/mol. Additionally, they are extended to intermediate strain states of an InGaN layer grown GaN. In contrast to Karpov[12] the elastic constants were taken from Wright.[22] They provide a consistent set of data and yield a better agreement between theoretical calculations and experimental results. Below each spinodal line there exists an unstable region for InGaN where phase separation should occur. With increasing strain up to 100% (i.e., the lateral lattice constant of InGaN is compressed to the lattice constant of GaN) the critical temperature (i.e., the maximum of the spinodal line) decreases and the unstable region shifts toward higher x. For a fully strained InGaN layer, the unstable region is significantly reduced. The critical temperature is 713 °C and phase separation is expected for lower temperatures. The limits within which strong phase separation would occur are $x_{\text{low}} = 0.71$ and $x_{\text{high}} = 0.87$ for a growth temperature of 600 °C and $x_{\text{low}} = 0.73$ and $x_{\text{high}} = 0.85$ for 650 °C, respectively. At very low temperature there is no, or only just, partial phase separation due to reduced kinetics.

In Fig. 3 the general patterns after phase separation are depicted for different x values and time steps and transferred to the case of InGaN. The patterns are calculated using the Cahn-Hilliard equation[21] and Eyres integration scheme.[23]

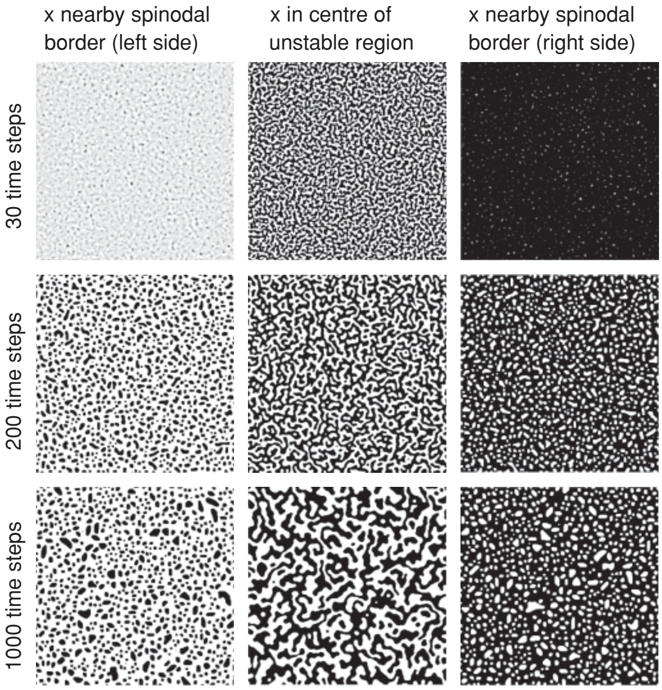

FIG. 3. General pattern after phase separation calculated for different time steps and for different initial x inside the unstable region (near the left border, in the center, near the right border). For the InGaN case the white regions would correspond to In$_{x_{\text{low}}}$Ga$_{1-x_{\text{low}}}$N and the black regions to In$_{x_{\text{high}}}$Ga$_{1-x_{\text{high}}}$N. For relatively higher and lower temperatures the number of time steps would decrease and increase, respectively, to obtain similar results.

For x being in the middle of the unstable region of the spinodal diagram, a meandering structure for both components would be obtained. An x close to the border of the unstable region would lead to a dot-like structure of one material embedded into the other material. However, two important facts are neglected in these patterns. First, due to the weak bond energy of In-N, indium has a high mobility on the surface or can be reevaporated into the gas phase. Second, the large lattice mismatch between InN and GaN would lead to a preferred Volmer-Weber growth mode of InN[24] or nearly 100% In-containing InGaN instead of a Frank-van-der-Merwe or Stranski-Krastanov growth mode. Therefore, it is expected that, after phase separation, the In$_{x_{\text{high}}}$Ga$_{1-x_{\text{high}}}$N phase would accumulate into large islands while the In$_{x_{\text{low}}}$Ga$_{1-x_{\text{low}}}$N phase would remain on the surface as it was formed after phase separation.

The strong dependence of the spinodal region onto the strain state of the material necessitates a consideration of the strain within a quantum dot which is coherently grown on an open surface. Therefore, finite element calculations were performed for quantum dots protruding from a flat surface. The calculations have been performed in cylindric coordinates assuming a circular quantum dot. The employed elasticity tensor was taken as before from Wright.[22] In Fig. 4 the strain state is depicted for four different aspect ratios of a coherent InGaN dot on a GaN surface. The strain state of the underlying GaN is not shown here, but is slightly tensile. Thus, the lower part of the quantum dot shows, in the center, a strain below 100% despite the pseudomorphic growth. The In content was

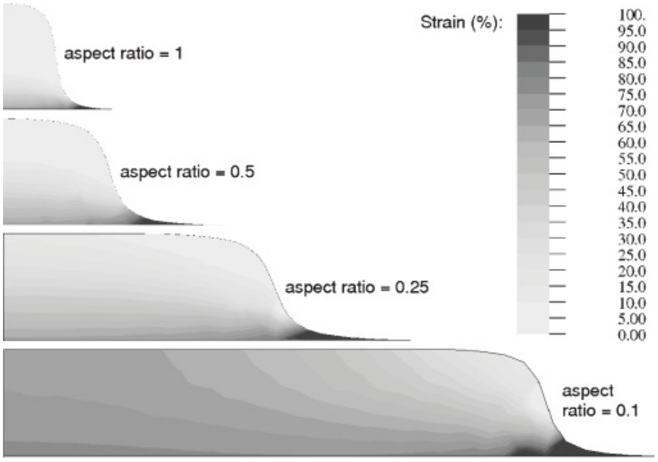

FIG. 4. Strain distribution for pseudomorphic $In_{0.648}Ga_{0.352}N$ QD protruding from a GaN substrate as a function of aspect ratio. Due to the symmetry, the right half is displayed only. The strain distribution is displayed in a gray scale between 0% and 100%. Due to the strain dependence of the spinodal region (Fig. 2) the decomposition has to be considered concerning the local strain.

chosen to $x = 0.648$. This value is the low-limit point of the binodal line at 600 °C for a 100% strained InGaN layer. The space in between the dots is free due to the high mobility of the In-rich regions and the accumulation into islands following the Volmer-Weber growth mode. It would represent the situation after a complete phase separation of a fully strained InGaN layer. For a small dot with an aspect ratio equal to 1 the mean strain in the dot is decreased. In that case, the corresponding strain-modified spinodal line (see Fig. 2) has to be taken into account. Thus, the $In_{x_{low}}Ga_{1-x_{low}}N$ material would be in the unstable region so that further phase separation would occur until the system reaches a stable x'_{low}. For a decreasing aspect ratio the strain increases (i.e., the InGaN composition is stabilized for larger dots).

IV. RESULTS AND DISCUSSION

A. Growth of uncapped InGaN structures

To investigate the evolution of a phase-separated thin InGaN layer, four samples were grown. Each $In_{0.82}Ga_{0.18}N$ layer was grown at 600 °C but the subsequent treatment was varied: sample A was directly cooled down to room temperature, sample B was annealed for four minutes at 600 °C, and samples C and D were annealed during a four-minute temperature ramp up to 700 and 750 °C, respectively. Afterwards the samples were cooled down to room temperature (RT). The growth parameters are summarized in Table I.

TABLE I. Parameters of uncapped InGaN samples A–D.

Uncapped Samples		
Sample ID	InGaN Growth Temperature	After Growth Procedure
A	600 °C	direct cooling
B	600 °C	4 min at 600 °C
C	600 °C	4 min ramp to 700 °C
D	600 °C	4 min ramp to 750 °C

In Fig. 5 the corresponding SEM images are depicted. Different features are visible on the surface of each sample: large dark and gray islands which are of truncated pyramidal shape as well as large bright islands of round shape (not found on sample A). In between the islands a dot-like and meandering structure is visible on the surface. Furthermore, some defects or pits were found (dark spots). For none of these samples are indium metal droplets present (see XRD measurements in Fig. 8). The evolution of the surface structure is in good agreement with the calculated phase-separation pattern in Fig. 3. For increasing temperature or time after growth, both enhancing the diffusion, the structure develops from a tight meandering and dot-like structure with a weak contrast to a large meandering and dot-like structure with a strong contrast.

In contrast to the calculated pattern in Fig. 3, large islands are found on the surface. Such kinds of islands are well known from the Volmer-Weber growth of InN on GaN.[24,25] The dark and gray truncated pyramidal-shaped islands seem to grow faster than the bright islands. For an annealing temperature of 750 °C the truncated pyramidal shaped islands start to shrink due to desorption, as is visible for sample D. Sample A in Fig. 5 does not show any of the round-shaped islands. In sample B a few of them with a small diameter are visible and in sample C their diameter is increased. It is expected that the slow growth of these islands is connected with the evolution process of the flat meandering structures. The SEM pictures indicate that two different InGaN phases are present on the surface which are formed during and after the growth of the InGaN layer.

A STEM measurement of sample C is shown in Fig. 6. One of the large truncated pyramidal-shaped islands is visible as well as the flat structures on the surface which are forming the meandering and dot-like structures. The flat structures have a height of 1–1.5 nm, which is in good agreement with the intended InGaN layer thickness. The large truncated pyramidal-shaped and round-shaped islands have a height and diameter of 20 nm and 40–50 nm, respectively. The large truncated pyramidal-shaped islands are found to form at dislocation sites while the round-shaped islands are expected not to be connected to a dislocation (not shown here). A high-In-content phase of about 80%–90% was found for both of these islands while a low-In content of around 20% is present in the flat structures.

In Fig. 7 the RT-PL measurements of the uncapped InGaN samples are presented. Strong InGaN PL in the visible range is observable for each sample. Nonradiative recombination of surface structures due to surface states lying in the band gap seems not to be a problem for the InGaN material system. Sample A shows bright luminescence at 520 nm (note that all PL features are superimposed by Fabry-Perot oscillations). With increasing annealing time or temperature the peak moves toward lower wavelengths. Sample D emits at 490 nm. The origin of the PL is attributed to the meandering and dot-like structures. With a band-gap bowing parameter of 2.5 eV[26] for InGaN and neglecting effects such as strain, the quantum-

Sample A:

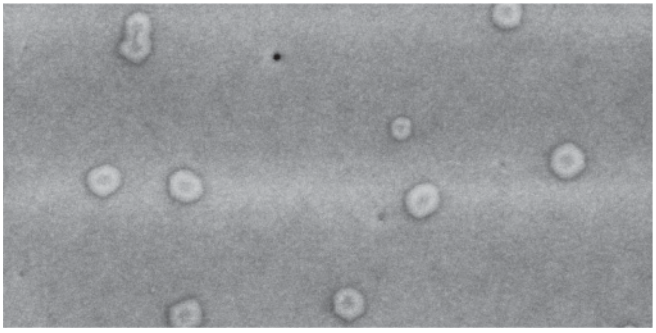

Sample B:

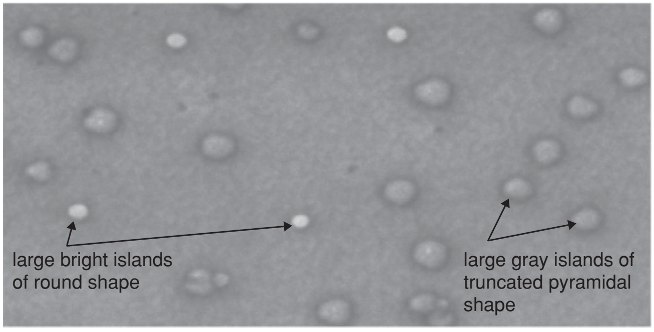

Sample C:

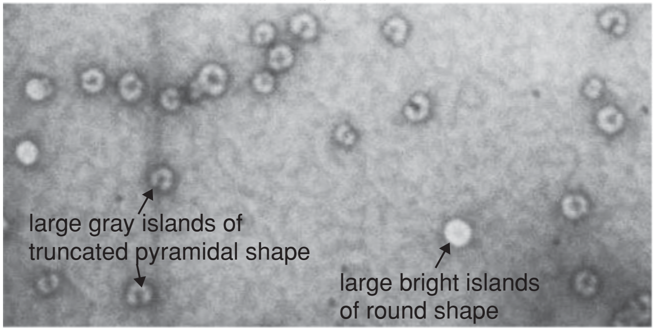

Sample D:

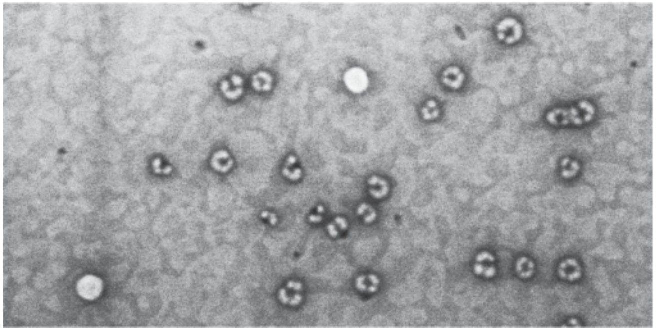

FIG. 5. SEM pictures (1 μm × 500 nm) of the surface of phase-separated InGaN layers with different annealing steps after growth (see also Table I).

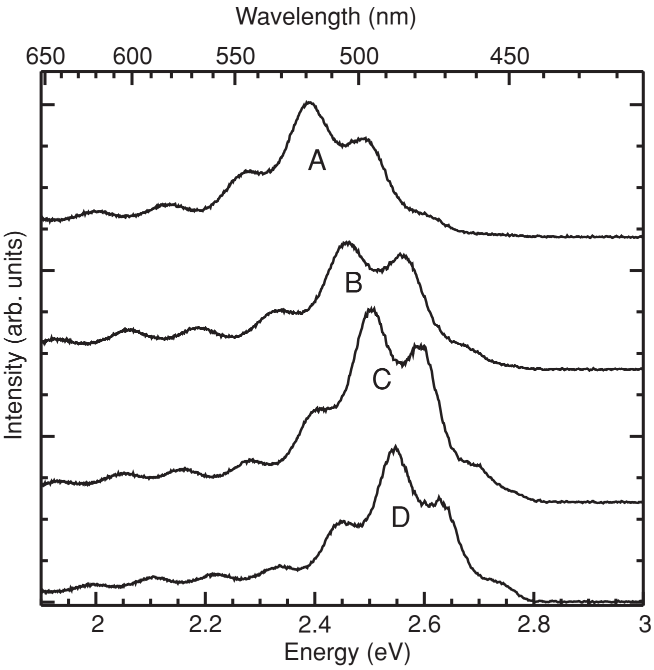

FIG. 7. RT-PL of the uncapped InGaN layers A–D. Strong PL from the QDs is visible from 2.3 to 2.7 eV, superposed by Fabry-Perot oscillations. At the low-energy side, sparse PL is visible originating from the yellow luminescence band.

confined Stark effect (QCSE) and quantum size effects, the band gap of, for example, $\mathrm{In}_{0.22}\mathrm{Ga}_{0.78}\mathrm{N}$ would be 2.47 eV. This is in good agreement with the emission wavelength of about 500 nm. Possible reasons for the observed blue shift are the asymptotic approximation to the binodal line or indium evaporation during annealing.

In Fig. 8 the XRD 2Θ-ω measurements along the (0002) reflex of the uncapped InGaN samples are shown. The simulated graph was obtained assuming a fully relaxed 20-nm-thick $\mathrm{In}_{0.97}\mathrm{Ga}_{0.03}\mathrm{N}$ layer. Each sample exhibits an InGaN phase with a very high-In content but not a pure InN phase. The In content for sample A and B is 97%, while it is reduced for sample C and D to 92.5%. The reduction is caused by the increased temperature during the thermal treatment after the growth of the InGaN layer, which leads to indium evaporation. The high-In content in the XRD signal is caused by the large islands.

In conclusion, the measurements demonstrate that strong phase separation occurs during and after the growth of the InGaN layer. Typical spinodal patterns are formed on the surface. Based on the spinodal phase diagram in Fig. 2, a decomposition of the $\mathrm{In}_{0.82}\mathrm{Ga}_{0.18}\mathrm{N}$ layer into a high- and a low-In-content phase is expected. The high-In phase accumulates

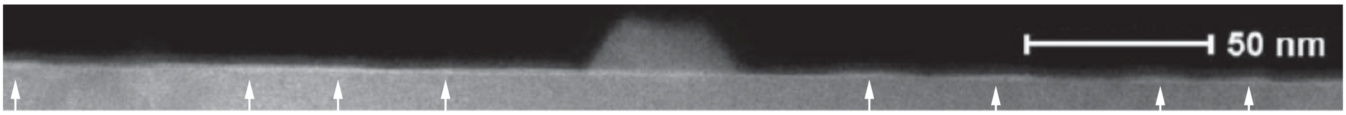

FIG. 6. STEM Z-contrast measurement of sample C. One of the large islands of truncated pyramidal shape with a high-In content (in the middle of the image) as well as the flat dot-like structures with a low-In content (marked with arrows) are visible on top of the GaN substrate.

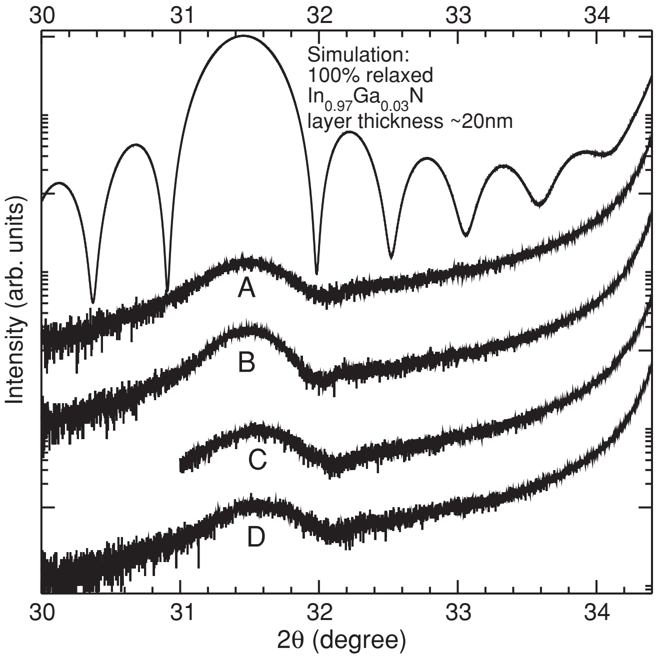

FIG. 8. XRD 2Θ-ω measurements along the (0002) reflex of the uncapped InGaN samples. InGaN with high-In content can be determined for each sample.

in the large relaxed islands due to the high mobility of indium. The binodal border for relaxed InGaN is 0.96, which is in excellent agreement with the $In_{0.97}Ga_{0.03}N$ phase found in XRD. The low-In-content phase exhibits a lower In content than expected from the spinodal phase diagram of the fully strained InGaN layer. A possible reason is already discussed in the theoretical section: a spinodal line for the lower strain state has to be considered after the relaxation of the free-standing InGaN dots. Thus, further decomposition would lead to a decrease of the In content. A detailed QD formation model based on phase separation will be presented in section E.

B. Influence of a GaN cap on InGaN structures

In order to investigate the characteristics of the phase-separated InGaN structures for further growth applications, two samples were grown using different GaN capping temperatures. Samples E and F are based on samples C and D, respectively. After deposition of the $In_{0.82}Ga_{0.18}N$ at 600 °C, the temperature was ramped in 4 min to 700 and 750 °C, respectively, and a 7-nm-thick GaN layer was grown. Afterward the temperature was increased to 820 °C to start with the high-temperature cap. During growth of this final capping the temperature was ramped to 1050 °C to obtain a high-quality GaN capping without the dissolution of the QD structures.[17]

The corresponding high-resolution STEM (HRSTEM) Z-contrast images and the evaluated In-concentration maps are shown in Fig. 9. A detailed description of the sample preparation for HRSTEM, the measurement, and the computation is given in 27. For both samples, the InGaN QD layer can be clearly seen as large compositional fluctuations in the first layer. The maximum In content was measured to be 18%. Furthermore, a second InGaN layer has formed in both samples with a lower In content of 8% (sample E) and 6% (sample F). The In distribution in this layer is homogeneous (i.e., a QW has formed above the QD layer). The QW in sample E has a thickness of a few monolayers and a distance of about 7 nm to the QD layer, while the QW in sample F has a thickness of about 7 nm and is directly connected to the QD layer. In the capped structures, none of the high-In-containing islands were found, meaning that they dissolve during the capping procedure. At 700 °C the In-rich InGaN islands are still stable and a pure GaN layer can be grown above the QD layer. During the temperature ramp from 700 to 820 °C the dissolution of the islands starts, the In spreads over the GaN surface, and the residuals are incorporated after the growth interruption of this temperature ramp at the beginning of the second GaN capping at 820 °C. This leads to the additional InGaN QW in case of this sample. The situation in sample F is different. During the growth of the GaN capping at 750 °C the In-rich InGaN islands already start to dissolve. Thus, the

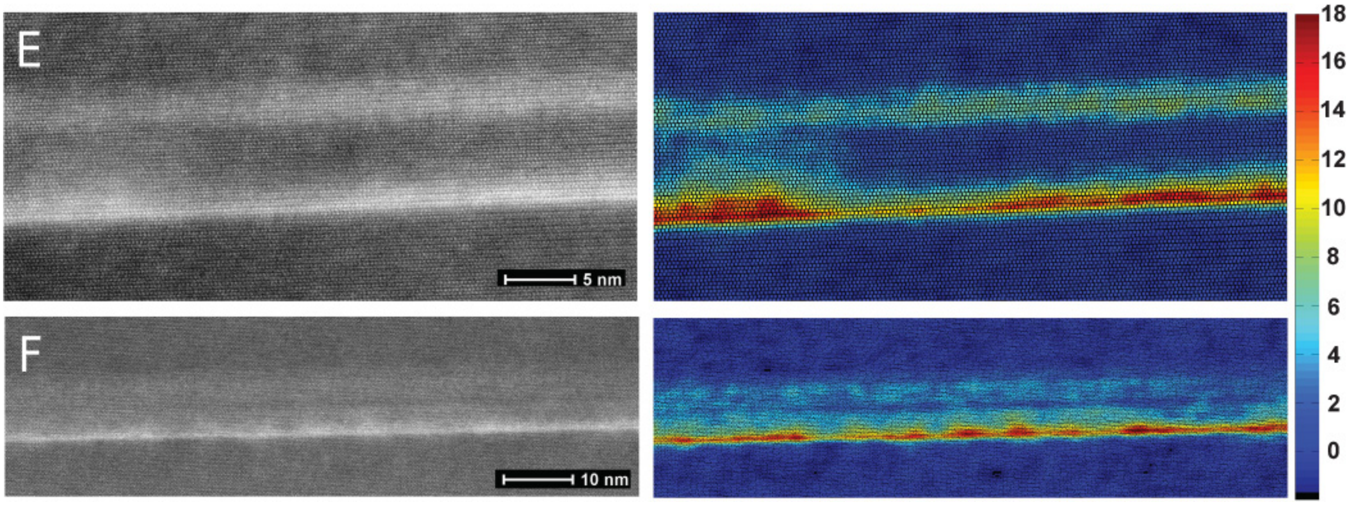

FIG. 9. (Color online) HRSTEM Z-contrast images (left) and the evaluated In-concentration maps (right) of GaN-capped phase-separated InGaN structures. Sample E (upper row) and F (lower row) were capped at 700 and 750 °C, respectively.

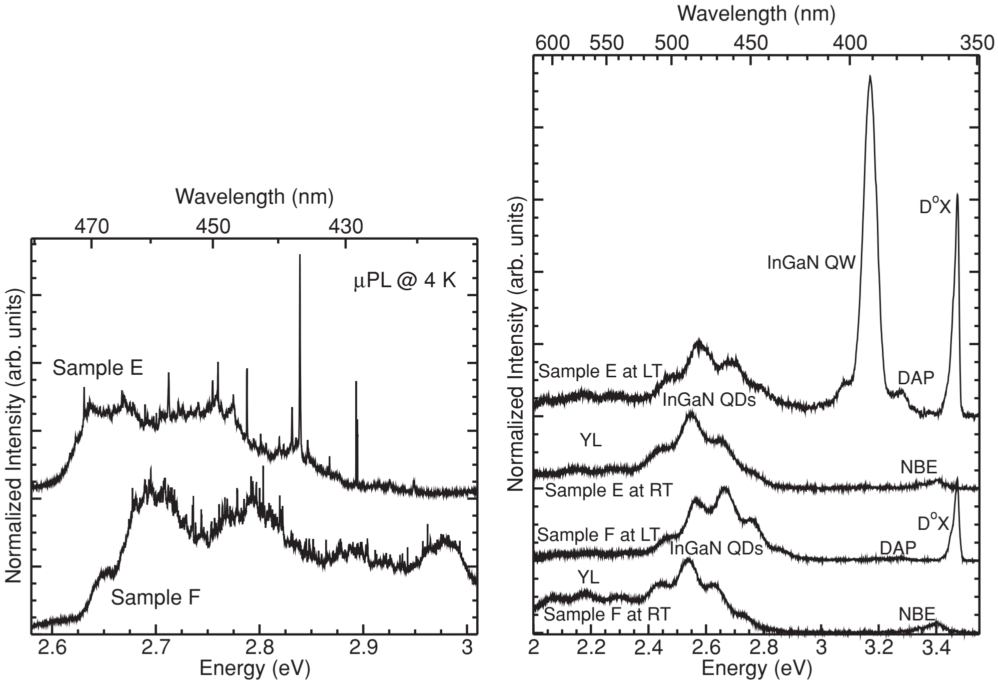

FIG. 10. μ-PL (left panel) and the normalized LT-PL to RT-PL comparison (right panel) of samples E and F. Sharp emission lines from the QDs can be identified in μ-PL. For each sample, broad yellow defect luminescence (YL) around 2.2 eV is visible. At LT, neutral-donor-bound exciton (D^0X) emission at 3.47 eV as well as donor-acceptor-pair recombination (DAP) at 3.25 eV and near-band-edge emission (NBE) at RT around 3.4 eV[28] are detectable.

In is incorporated homogeneously during the whole growth of the first GaN capping.

Optical investigations on sample E and F were performed. In Fig. 10 the μ-PL spectra as well as the RT-PL in comparison to low-temperature (LT) PL are shown. Sharp emission lines for both samples can be clearly identified in μ-PL; that is, the InGaN QDs found in TEM in Fig. 9 are optically active. For sample E at LT the QD emission is visible at 2.55 eV but the QW at 3.15 eV dominates the spectrum. At RT the QD emission is still visible while the intensity of the QW has dropped dramatically. This shows one of the advantages of QDs in comparison to a QW: the luminescence efficiency of QDs at RT is much higher than that of a QW. Due to the high mobility of the carriers in the QW at RT they recombine nonradiatively at defects. The carriers in the QD are confined in three dimensions, thus, nonradiative recombination at defects is prevented. For sample F essentially no QW emission is visible; that is, the QW acts as a transport layer only and the carriers relax from the QW into the QDs. The radiative recombination takes place in the QDs only. The difference between the emission energy of the μ-PL and macro-PL spectra is due to the excitation density in μ-PL measurements, which is around three orders of magnitude higher than in macro-PL measurements. This causes a high carrier density which leads to a screening of the piezoelectric fields and a reduction of the QCSE.[29] Thus, the characteristic QD emission is distinctly blue shifted.

C. Control of the QD density

It is expected from the correlation between temperature and diffusion length that the QD size and density could be controlled, as is shown in 16: with increasing temperature the density of QDs decreases. Furthermore, the size and density should be dependent on the In content in the unstable InGaN layer. An increase in the In content leads to a decrease in size and density of the In-poor InGaN regions. The AFM measurement in Fig. 11 shows the surface of a sample with a decomposed InGaN layer grown at 650 °C. The same features as in Fig. 5 are visible. Islands occur with small and large diameters but with the same height of around 20 nm. The flat InGaN QDs with a height of 1–1.5 nm are visible on the surface. They are well separated from each other and no meandering structure is visible. The size is increased and the density is reduced compared to the samples shown in Fig. 5. This is due to the increased temperature as well as to the fact that, at 650 °C, the unstable $In_{0.82}Ga_{0.18}N$ layer is closer to the border of the spinodal line (see Fig. 2). RT-PL emission at 500 nm is detectable as well as an $In_{0.97}Ga_{0.03}N$ phase in XRD (not shown here). Spinodal decomposition into two different InGaN phases takes place at 650 °C, too.

In Fig. 12 the PL spectra of samples with $In_{0.82}Ga_{0.18}N$ layers grown at 600, 650, and 700 °C are shown. With increasing growth temperature the PL intensity decreases. The decrease correlates with a reduction of the QD density. In Table II the density of the QDs is given for different growth temperatures. The QD density was determined by counting the number of spectrally sharp emission lines from μ-PL spectra of a defined mesa structure. By adjusting the growth temperature of the InGaN layer, the density can be controlled over three orders of magnitude. The results show that it is possible to grow different QD densities suitable for any kind of application: a

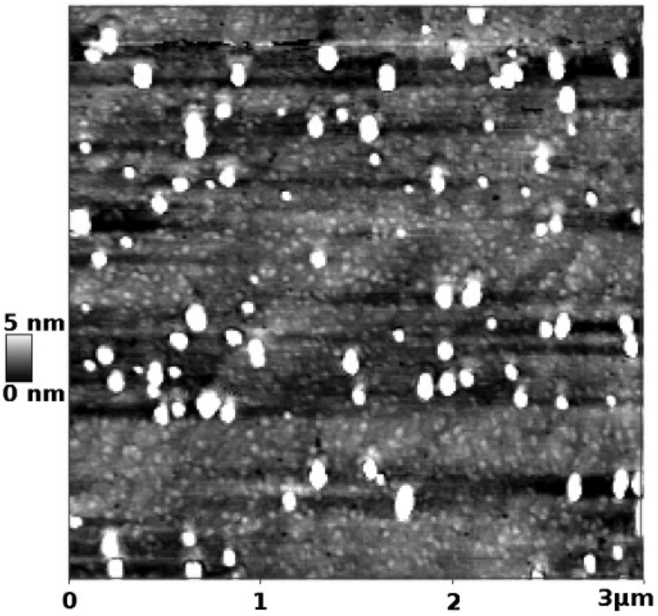

FIG. 11. AFM of a phase-separated InGaN layer grown at 650 °C. The high-In-containing islands have a height of 20 nm. The scale height was set to 5 nm to have a better contrast for the flat and small dots on the surface.

high QD density for LD and LED structures, and a low QD density for single-photon emitters.

D. Variation of In content of InGaN layer

TABLE II. Density of QDs determined by counting spectrally sharp emission lines in the μ-PL spectra from a mesa structure.

InGaN Growth Temperature	Number of Sharp Emission Lines
600 °C	1×10^{11} cm^{-2}
650 °C	6×10^{9} cm^{-2}
700 °C	2×10^{8} cm^{-2}

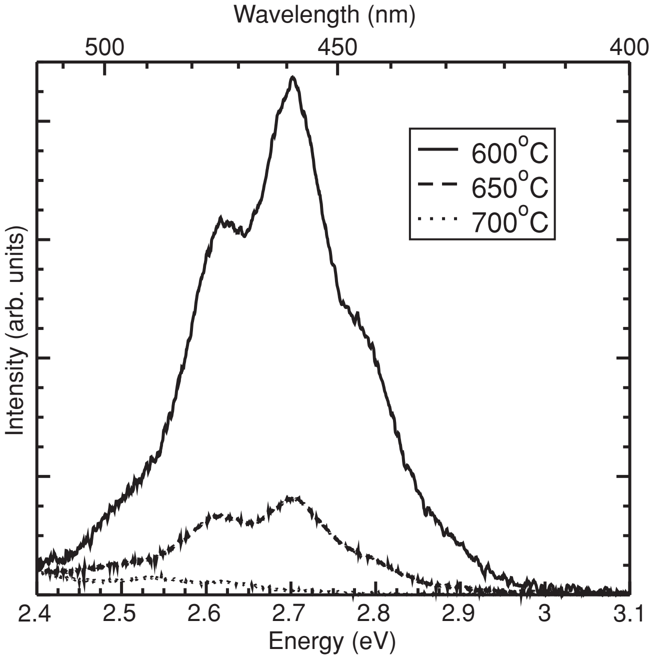

FIG. 12. RT-PL of samples with different growth temperatures for the InGaN layer.

To investigate the influence of an In$_x$Ga$_{1-x}$N layer with x inside and outside the unstable region of a modified spinodal phase diagram for the fully strained case, samples with $x = 0.73$ (sample G), 0.78 (H), 0.82 (I), 0.87 (J), and 0.92 (K) were grown at a temperature of 650 °C. The samples were capped with a 7-nm In$_{0.09}$Ga$_{0.91}$N layer at 700 °C and a 36-nm GaN layer at 820 °C. An overview of the samples is given in Table III. The compositions of the InGaN layers of the samples G, J, and K are outside and the samples H and I are inside the unstable region for a fully strained InGaN layer (see Fig. 2). The PL spectra recorded at RT are given in Fig. 13(a). Corresponding temperature-dependent measurements are displayed in Fig. 13(b). Samples G and K show emission around 3 eV. With increasing temperature a strong decrease in PL intensity is observed and the RT-PL to LT-PL is smaller than 0.005. Such an intensity loss is typical for a QW emission.[30] The emission energies at RT of samples H, I, and J are 2.65, 2.66, and 2.82 eV, respectively. This finding is in contrast to the expectation of a lowering band-gap energy with increasing In content. The RT-PL to LT-PL ratio for samples H and I is higher compared to the other samples and amounts to 0.067 and 0.062, respectively. These relatively high values are a characteristic property of QDs. For sample J a medium decrease in intensity is observed, the RT-PL/LT-PL ratio is 0.013. The samples with x in the unstable region of the spinodal phase diagram show a QD-like PL behavior; that is, sharp emission lines in μ-PL and a weak decrease of intensity in temperature-dependent PL measurements up to RT are observed. In contrast, samples with x placed in the metastable or stable region show a QW-like behavior. It is assumed that, for these samples, no phase separation occurs.

The reason for the optical characteristics of the sample with $x = 0.87$, which shows properties in between a QD and a QW, is thought to be caused by In desorption after the growth of the InGaN layer. Therefore, the In content in InGaN can slide into the unstable region and phase separation can happen. In such a case the In content is near the $x = 0.852$ border, and these QDs are very small, as predicted in 16. For smaller InGaN QDs, the elastic relaxation process is increased as already described in the theoretical section. This would lead to a lower In content in the QDs. Another effect is caused by the size of the QD. Due to the quantum size effect, the distance of the energy levels

TABLE III. Main parameters of samples G–K.

Sample ID	InGaN Growth Temperature	x in In$_x$Ga$_{1-x}$N	1. GaN Cap Temperature
G	650 °C	0.73	700 °C
H	650 °C	0.78	700 °C
I	650 °C	0.82	700 °C
J	650 °C	0.87	700 °C
K	650 °C	0.92	700 °C

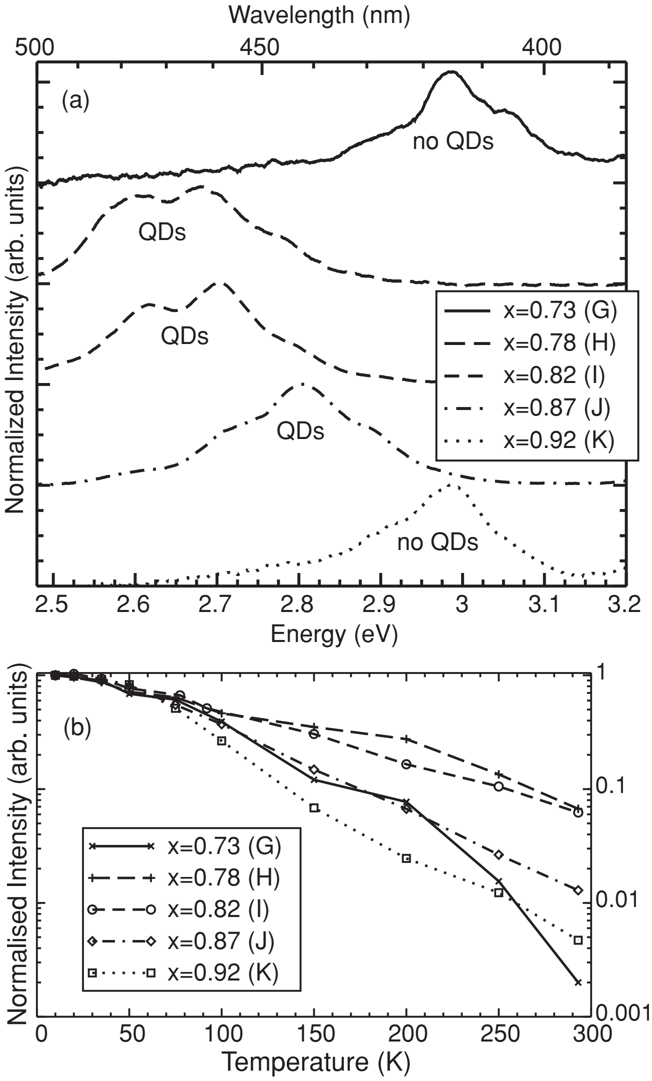

FIG. 13. (a) PL spectra recorded at RT for samples G–K with different x in the $In_xGa_{1-x}N$ layer. (b) Corresponding temperature-dependent integrated PL intensity.

between electrons and holes is increased with decreasing the size of a QD. This effect is also responsible for the blue shift in the PL. Furthermore, for smaller QDs the energy levels are shallow and an excited electron can escape easier from the InGaN QD into the surrounding (In)GaN when thermal energy is provided.

E. QD formation model

It was shown that phase separation occurs for a strained InGaN layer when the composition is set to the unstable region below the spinodal line considering strain. In-poor QD-like structures and In-rich islands are found on the surface. In agreement with the theoretical and experimental results an InGaN QD formation model is proposed. The growth of QDs takes the path depicted in Figs. 14(a)–14(f). After the growth of a fully strained $In_aGa_{1-a}N$ layer [Fig. 14(a)] phase separation occurs [Fig. 14(b)] when the composition a is within the unstable spinodal region for a strain state of 100% (see Fig. 2). Areas with In-poor $In_bGa_{1-b}N$ and In-rich $In_cGa_{1-c}N$ are found on the surface in a configuration as in Fig. 3. The In-rich material has a high surface mobility and can accumulate to large islands (see Figs. 5 and 11) or desorbs due to the low thermal stability. Separated $In_bGa_{1-b}N$ islands remain on the surface [Fig. 14(c)] which can partly elastically relax [Fig. 14(d)]. This changes the Gibbs free energy and thus expands the region of instable compositions, as is seen for material with a lower strain state (Fig. 2). The $In_bGa_{1-b}N$ is unstable; a further phase separation occurs into even In-poorer $In_dGa_{1-d}N$ [Fig. 14(e)]. As the upper limit of the spinodal region does not change too much with the strain state, the In-rich $In_eGa_{1-e}N$ behaves similar to the above-discussed phase c. Finally, the $In_dGa_{1-d}N$ regions form the QDs [Fig. 14(f)], which have a band-gap energy corresponding to an emission wavelength in the green to blue visible region (see Fig. 7). However, these different phases of quantum dot formation need not consecutively follow each other, but can take place in parallel. This model is in good accordance with the experimental data presented in this paper.

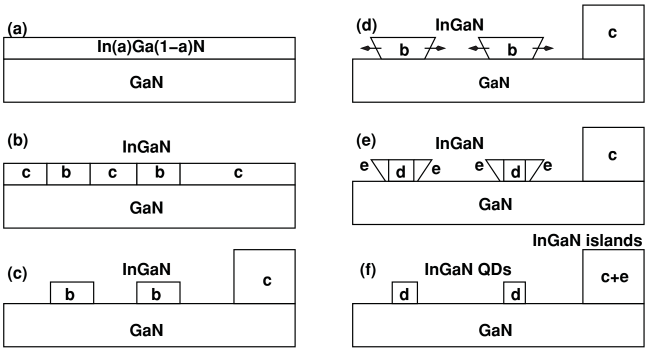

FIG. 14. QD formation model based on spinodal decomposition and relaxation of coherent dots or islands. Each step of the model is explained in the text.

V. SUMMARY

In conclusion, a narrow growth window depending on x in $In_xGa_{1-x}N$ is found in which strong phase separation due to spinodal and binodal decomposition and the formation of InGaN QDs and InGaN islands takes place. The growth window is connected to the unstable region below the spinodal line for the case of a fully strained InGaN layer. Uncapped InGaN structures were grown in MOVPE and typical spinodal patterns are visible by SEM. In-rich and In-poor InGaN structures were found. The InGaN QDs with a low-In content were measured in TEM and sharp emission lines in μ-PL were detected. The In-rich InGaN islands dissolve during the growth of the GaN capping at elevated temperatures and form an additional InGaN QW. The density of QDs can be adjusted in a range between 10^8–10^{11} cm^{-2} by setting the growth temperature. Based on spinodal decomposition a QD formation model was developed.

ACKNOWLEDGMENTS

This project has been funded by the German research society DFG within project number FOR 506 and the Bundesministerium für Bildung und Forschung (BMBF) project QPENS.

[*] ctessarek@ifp.uni-bremen.de

[1] K. Sebald, M. Seyfried, J. Kalden, J. Gutowski, H. Dartsch, C. Tessarek, T. Aschenbrenner, S. Figge, C. Kruse, and D. Hommel, Appl. Phys. Lett. **96**, 251906 (2010).

[2] J. Kalden, C. Tessarek, K. Sebald, S. Figge, C. Kruse, D. Hommel, and J. Gutowski, Nanotechnology **21**, 015204 (2010).

[3] R. A. Oliver, G. A. D. Briggs, M. J. Kappers, C. J. Humphreys, S. Yasin, J. H. Rice, J. D. Smith, and R. A. Taylor, Appl. Phys. Lett. **83**, 755 (2003).

[4] Q. Wang, T. Wang, J. Bai, A. G. Cullis, P. J. Parbrook, and F. Ranalli, J. Appl. Phys. **103**, 123522 (2008).

[5] D. Queren, A. Avramescu, G. Brüderl, A. Breidenassel, M. Schillgalies, S. Lutgen, and U. Strauß, Appl. Phys. Lett. **94**, 081119 (2009).

[6] T. Miyoshi, S. Masui, T. Okada, T. Yanamoto, T. Kozaki, S. Nagahama, and T. Mukai, Appl. Phys. Express **2**, 062201 (2009).

[7] I.-H. Ho and G. B. Stringfellow, Appl. Phys. Lett. **69**, 2701 (1996).

[8] M. V. Maximov, A. F, Tsatsul'nikov, B. V. Volovik, D. A. Bedarev, A. E. Zhukov, A. R. Kovsh, N. A. Maleev, V. M. Ustinov, P. S. Kop'ev, Zh. I. Alferov, R. Heitz, N. N. Ledentsov, and D. Bimberg, Phys. E **7**, 326 (2000).

[9] N. N. Ledentsov and D. Bimberg, J. Cryst. Growth **255**, 68 (2003).

[10] T. Kuykendall, P. Ulrich, S. Aloni, and P. Yang, Nature Mater. **6**, 951 (2007).

[11] M. I. Richard, M. J. Highland, T. T. Fister, A. Munkholm, J. Mei, S. K. Streiffer, C. Thompson, P. H. Fuoss, and G. B. Stephenson, Appl. Phys. Lett. **96**, 051911 (2010).

[12] S. Y. Karpov, MRS Internet J. Nitride Semicon. Res. **3**, 16 (1998).

[13] M. J. Cherng, G. B. Stringfellow, and R. M. Cohen, Appl. Phys. Lett. **44**, 67 (1984).

[14] N. Motta, A. Balzarotti, P. Letardi, A. Kisiel, M. T. Czyzyk, M. Zimnal-Starnawska, and M. Podgorny, J. Cryst. Growth **72**, 205 (1985).

[15] A. Koukitu, Y. Kumagai, and H. Seki, J. Crystal Growth **221**, 743 (2000).

[16] T. Okumura, M. Ishida, and T. Kamikawa, Jpn. J. Appl. Phys. **39**, 1044 (2000).

[17] C. Tessarek, T. Yamaguchi, S. Figge, and D. Hommel, Phys. Status Solidi C **6**, S561 (2009).

[18] T. Yamaguchi, K. Sebald, H. Lohmeyer, S. Gangopadhyay, J. Falta, J. Gutowski, S. Figge, and D. Hommel, Phys. Status Solidi C **3**, 3955 (2006).

[19] T. Saito and Y. Arakawa, Phys. Rev. B **60**, 1701 (1999).

[20] T. Yamaya, Y. Kangawa, K. Kakimoto, and A. Koukitu, Jpn. J. Appl. Phys. **48**, 088004 (2009).

[21] J. W. Cahn and J. E. Hilliard, J. Chem. Phys. **28**, 258 (1958).

[22] A. F. Wright, J. Appl. Phys. **82**, 2833 (1997).

[23] D. Eyre, *Symposium on Computational and Mathematical Models of Microstructural Evolution at the 1998 MRS Spring Meeting* (San Francicso, CA, 1998), MRS Symp. Proc. **529**, 39 (1998).

[24] C. Meissner, S. Ploch, M. Leyer, M. Pristovsek, and M. Kneissel, J. Cryst. Growth **310**, 4959 (2009).

[25] W.-H. Chang, W.-C. Ke, S.-H. Yu, L. Lee, C.-Y. Chen, W.-C. Tsai, H. Lin, W.-C. Chou, M.-C. Lee, and W.-K. Chen, J. Appl. Phys. **103**, 104306 (2008).

[26] V. Y. Davydov, A. Klochikhin, V. V. Emtsev, D. A. Kurdyukov, S. V. Ivanov, V. A. Vekshin, F. Bechstedt, J. Furthmuller, J. Aderhold, J. Graul, A. V. Mudryi, H. Harima, A. Hashimoto, A. Yamamoto, and E. E. Haller, Phys. Status Solidi B **234**, 787 (2002).

[27] A. Rosenauer, T. Mehrtens, K. Müller, K. Gries, M. Schowalter, S. Bley, C. Tessarek, D. Hommel, K. Sebald, M. Seyfried, J. Gutowski, A. Avramescu, K. Engl, S. Lutgen (unpublished).

[28] M. A. Reshchikov and H. Morkoc, J. Appl. Phys. **97**, 061301 (2005).

[29] A. F. Jarjour, R. A. Oliver, A. Tahraoui, M. J. Kappers, R. A. Taylor, and C. J. Humphreys, Superlatt. Microstruct. **43**, 431 (2008).

[30] A. Chahboun, M. I. Vasilevsky, N. V. Baidus, A. Cavaco, N. A. Sobolev M. C. Carmo, E. Alves, and B. N. Zvonkov, J. Appl. Phys. **103**, 083548 (2008).